A semi-analytical bearing model considering outer race flexibility for model based bearing load monitoring

Kerst, Stijn; Shyrokau, Barys; Holweg, Edward

DOI
10.1016/j.ymssp.2017.11.008

Publication date
2018

Document Version
Final published version

Published in
Mechanical Systems and Signal Processing

Citation (APA)
Kerst, S., Shyrokau, B., & Holweg, E. (2018). A semi-analytical bearing model considering outer race flexibility for model based bearing load monitoring. *Mechanical Systems and Signal Processing*, *104*, 384-397. https://doi.org/10.1016/j.ymssp.2017.11.008

Mechanical Systems and Signal Processing 104 (2018) 384–397

Contents lists available at ScienceDirect

Mechanical Systems and Signal Processing

journal homepage: www.elsevier.com/locate/ymssp

A semi-analytical bearing model considering outer race flexibility for model based bearing load monitoring

Stijn Kerst *, Barys Shyrokau, Edward Holweg

Department of Cognitive Robotics, Faculty of Mechanical, Maritime and Materials Engineering, Delft University of Technology, The Netherlands

ARTICLE INFO

Article history:
Received 3 March 2017
Received in revised form 30 October 2017
Accepted 3 November 2017
Available online 11 November 2017

Keywords:
Rolling bearing
Load reconstruction
Modelling
Condition monitoring

ABSTRACT

This paper proposes a novel semi-analytical bearing model addressing flexibility of the bearing outer race structure. It furthermore presents the application of this model in a bearing load condition monitoring approach. The bearing model is developed as current computational low cost bearing models fail to provide an accurate description of the more and more common flexible size and weight optimized bearing designs due to their assumptions of rigidity. In the proposed bearing model raceway flexibility is described by the use of static deformation shapes. The excitation of the deformation shapes is calculated based on the modelled rolling element loads and a Fourier series based compliance approximation. The resulting model is computational low cost and provides an accurate description of the rolling element loads for flexible outer raceway structures. The latter is validated by a simulation-based comparison study with a well-established bearing simulation software tool. An experimental study finally shows the potential of the proposed model in a bearing load monitoring approach.

1. Introduction

Rolling bearings are commonly used machine elements permitting rotational motion of shafts. They are applied in a wide range of applications from simple commercial devices to highly complex mechanisms. As in many facets of mechanical engineering increasing demands are put on rolling bearings. Besides development in areas as for instance lubrication, sealing and fatigue life, special interest lies in lifetime prediction and fault detection in order to avoid unnecessary upkeep and breakdowns. This latter is of utmost importance as bearings are usually essential machinery components [1].

A wide variety of damage modes might cause premature bearing failure. Examples are numerous and include manufacturing errors, excessive or improper loading, misalignment, overheating, corrosion and lubrication failure [2]. Next to premature failure modes a bearing will furthermore eventually fail in time due to fatigue of the bearing material. As bearing failure is one of the most common reasons for machinery breakdowns [3] bearing condition monitoring is an active field of research.

Incipient bearing failure is often characterized by a local defect on one of the bearing components and the detection of such defects is the main focus of condition monitoring [4]. Various approaches based on vibration, acoustic emission, sound pressure, lubrication and thermal analysis have been developed for detection and diagnosis of bearing defects [5–8]. Vibration analysis is the most common approach in both literature and industry and is based on various types on analysis in the

* Corresponding author at: Faculty of Mechanical, Maritime and Materials Engineering, Delft University of Technology, Mekelweg 2, 2628 CD Delft, The Netherlands.
E-mail address: s.m.a.a.kerst@tudelft.nl (S. Kerst).

https://doi.org/10.1016/j.ymssp.2017.11.008
0888-3270/

vibration spectrum [9,10]. Advantages of these approaches relate to the basic sensory equipment needed, their effectiveness and the ability to detect the location of the defect [11,12]. Acoustic emission approaches have also been successfully applied and studies show that it allows for detection subsurface cracks before spalling occurs [13,14]. The approach itself however is considerably more extensive as sensor location is crucial and signal processing is more complex. In lubrication analysis on- or off-line debris detection is applied on the bearing lubricant [15]. Major benefit of this approach is the independence of background noise and machine operating conditions, however its drawbacks include processing complexity and classification. Thermal analysis based condition monitoring approaches [16,17] provide similar advantages and drawbacks. For improved fault diagnostics combinations of different approaches and analysis techniques can be applied [18,19].

Excessive or improper loading and bearing misalignment relate to a considerable portion of local defect initiation and growth. Continuous load monitoring could detect these damage modes and therefore help to avoid bearing failures. Next to that it could serve as a valuable control input for system control [20]. Load monitoring at the bearing level can be classified in deformation and displacement based approaches. The deformation based approaches are founded on strain measurement at the non-rotating bearing outer-ring by the use of strain gauges or optical fibres [21–26]. Displacement load monitoring approaches are based on the measurement of the relative displacement of inner- to outer ring by the use of hall effect, eddy-current or capacitive sensors [27–29]. In both load monitoring principles the measured physical quantities are translated to the bearing loading by empirical methods as least squares fitting [30,31] or artificial neural networks [32]. In the deformation based approach this last step however is extremely challenging as the relationship between measured strain and loading is highly non-linear [23]. To capture this non-linearity adequately a model based approach is preferred.

Modelling bearing behaviour for real-time load monitoring is a complex issue as an accurate description of the behaviour is desired whilst computing power is limited. Size and weight considerations during system and bearing development often results in flexible structures that deform considerably even at standard operational loads. This leads to altered load distributions, deflections, contact stresses and fatigue endurance compared to calculations using rigid assumptions. Considering the structural bearing deformation is thus of paramount importance for accurately describing bearing behaviour. Well established computational low cost analytical bearing models [1,33,34] are thus inapplicable due to their assumptions of rigidity. The usage of Finite Element Modelling [35], allowing for an accurate description of the flexibility, on the other hand is too computationally costly. Model reduction of for instance contact mechanics [36–38] or deformation behaviour [39] furthermore does not provide sufficient computational gain for real-time calculation. The most appropriate modelling approach for real-time load monitoring is therefore found in-between the analytical and Finite Element based approaches in the form of a semi-analytical flexible bearing model [40–42].

The semi-analytical flexible bearing models are formed by extension of traditional rigid analytical modelling by a semi-analytical description of the bearing outer-ring deformation. The in-plane deformation or ovalization of the outer-raceway is described using a Fourier series representation. The Fourier coefficients are either analytically derived from Timoshenko's theory [40–42] or determined based on a Finite Element Analysis of the structure [42]. Main limitation of the current modelling approaches is the assumption of axisymmetric geometries. This limits the applicability in real-life situations as bearing housings in general do not comply to this strict geometric limitation.

To accurately include the structural deformation of any outer-ring housing geometry at low computational cost in this paper a novel semi-analytical bearing model is proposed. By the use of static deformation shapes and a Fourier series based compliance approximation an accurate and efficient representation of the raceway flexibility is obtained. The Fourier coefficients are determined a priori by the use of a Finite Element study on the outer-race structure according to a simple procedure. Simulation studies show that the model is able to accurately describe the rolling element loads when significant structural bearing deformation is present. The model is furthermore implemented in an experimental study to show its potential in load monitoring.

2. Bearing model

In this Section the proposed bearing model is developed. The following important assumptions and simplifications are applied: (i) as low speeds are considered the effect of centrifugal forces is neglected, (ii) both friction and cage interaction forces are neglected as they are insignificant compared to the rolling element normal loads and (iii) only radial deformation of the outer race is considered as the axial component in general is considerably less excited and influential. Furthermore some minor assumptions are provided within the work itself.

2.1. Coordinate systems

For the development of the bearing model two coordinate systems are used, namely a Cartesian and cylindrical system. Fig. 1 shows the groove curvature loci of inner and outer raceway and their associated parameters in the Cartesian x, y, z space. The origin of the Cartesian space is located at the inner ring reference point at its undisplaced position. The x and y-axis are respectively the vertical and horizontal radial bearing direction whilst the z-axis is aligned with the bearing axis. All rigid body displacements and bearing loads are defined in this Cartesian system.

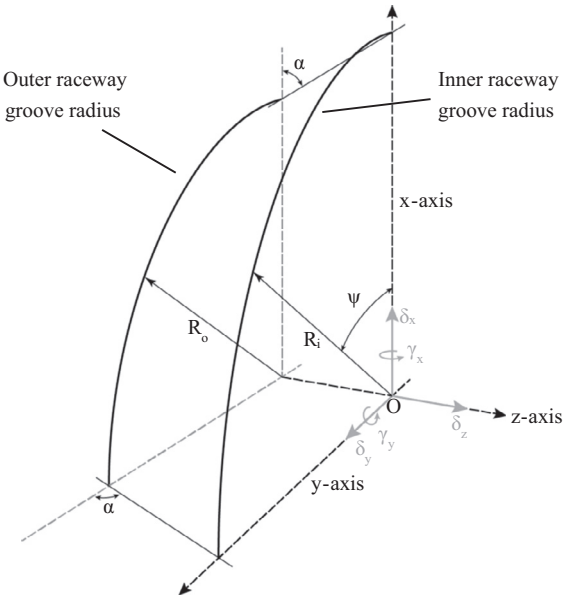

Fig. 1. Loci of raceway groove curvature centres in Cartesian space.

A cylindrical r, ψ, z system is used for description of the raceway approach and calculation of the rolling element loads. The origin and z-axis align with the Cartesian system and ψ is the angle between the r-axis and the Cartesian x-axis with $[-\pi < \psi \leq \pi]$.

2.2. Definition of element load and operating angle

The element loads are defined based on the deflection of the rolling elements by both raceways [1]. The ball-raceway normal load Q as function of deflection is defined as:

$$Q = K_n \delta_n^{3/2} \tag{1}$$

where K_n is the load–deflection factor and δ_n the sum of the normal approaches between rolling element and raceways. The load–deflection factor depends on the materials and curvatures of the bodies in contact and in this paper is calculated in line with [1]. The normal approach δ_n is defined as the approach of the curvature loci of the raceway grooves according to:

$$\delta_n = s - A \tag{2}$$

where s is the inner and outer race curvature loci distance and A is the curvature loci distance at first contact (and zero loading) defined as:

$$A = r_i + r_o - D \tag{3}$$

where r_i and r_o are respectively the inner and outer raceway groove curvature radii and D is the ball diameter. The inner and outer race curvature centre positions in the radial (R_i and R_o) and axial (Z_i and Z_o) direction are presented in Fig. 2.

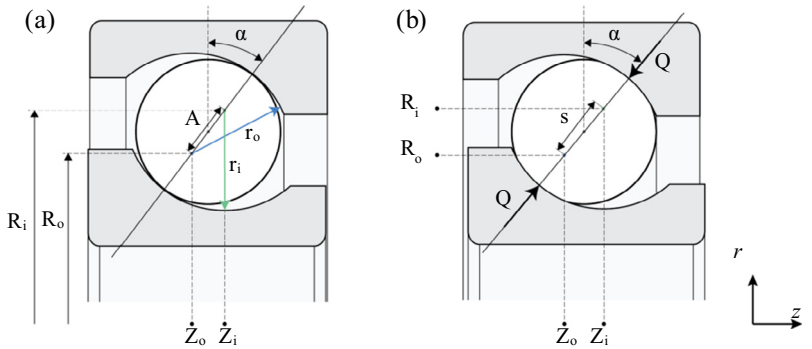

Fig. 2. Radial ball bearing section view including relevant variables for (a) unloaded and (b) loaded conditions.

The overlap of the inner and outer groove raceway curvature centres is defined as:

$$s = \left[(R_i - R_o)^2 + (Z_i - Z_o)^2\right]^{1/2} \tag{4}$$

and the operating contact angle α as:

$$\tan(\alpha) = \frac{Z_i - Z_o}{R_i - R_o} \tag{5}$$

2.3. Rigid body displacements of inner-raceway

In line with common literature [1] it is chosen to fix the outer ring in space whilst the inner ring is allowed for rigid body displacements. All five relevant Degrees Of Freedom (DOF) are captured in the displacement vector that is attached to the inner ring at origin O as shown in Fig. 1. The displacement vector is defined as:

$$\boldsymbol{\delta}_D = \langle \delta_x \quad \delta_y \quad \delta_z \quad \gamma_x \quad \gamma_y \rangle^T \tag{6}$$

where δ_x, δ_y, δ_z are the axial translations, γ_x and γ_y are the rotations over the x and y-axis respectively. With the assumption of small angles the displacement vector defines the inner raceway groove curvature loci as a function of the bearing azimuth ψ in radial and axial direction according to:

$$R_i(\psi) = R_{i0} + \delta_x \cos(\psi) + \delta_y \sin(\psi) \tag{7}$$

$$Z_i(\psi) = Z_{i0} + \delta_z + R_{i0}\gamma_x \sin(\psi) + R_{i0}\gamma_y \cos(\psi) \tag{8}$$

where R_{i0} is the radius of locus of the inner raceway groove curvature centre and Z_{i0} is the initial axial displacement of the groove curvature centre.

2.4. Outer raceway modelling

The raceway deformation is accommodated by the use of a semi-analytical approximation model. The proposed implementation extends the classical static definition of the outer raceway groove curvature loci in radial direction:

$$R_o(\psi) = R_{o0} + u_r(\psi) \tag{9}$$

where R_{o0} is the static radius of the curvature loci and u_r the deformation of the raceway. For reasons of clarity the explicit description of the latter will be discussed in Section 3. As no deformation in axial direction is considered, the axial position of the groove curvature loci Z_o is static and equals Z_{o0}.

2.5. Rolling element forces and bearing forces and moments

The rigid body displacement vector $\boldsymbol{\delta}_D$ and outer race flexibility model define the rolling element normal load Q and operating contact angle α for all bearing azimuth positions. The normal load Q can be resolved in radial and axial components:

$$Q_r = Q\cos(\alpha) \tag{10}$$

$$Q_z = Q\sin(\alpha) \tag{11}$$

where Q_r and Q_z are the radial and axial load respectively. Now introducing the index n for representation of the nth rolling element and its corresponding ball azimuth position ψ_n, the bearing forces and moments can be described by summation over all rolling elements:

$$\begin{cases} F_x = \sum\limits_{n=1..N_{re}} Q_{rn}\cos(\psi_n) \\ F_y = \sum\limits_{n=1..N_{re}} Q_{rn}\sin(\psi_n) \\ F_z = \sum\limits_{n=1..N_{re}} Q_{zn} \\ M_x = \sum\limits_{n=1..N_{re}} Q_{zn}R_m\sin(\psi_n) \\ M_z = \sum\limits_{n=1..N_{re}} Q_{zn}R_m\cos(\psi_n) \end{cases} \tag{12}$$

where N_{re} is the total number of rolling elements and R_m is the bearing pitch radius which equals $(R_i + R_o)/2$.

3. Raceway deformation model

Flexibility of the outer raceway is implemented by the use of a semi-analytical approximation of the static elastic radial bearing deformation. The deformation of any point on the raceway due to a single rolling element load can be deduced from the static components of the equation of motion:

$$u_r(\psi) = K^{-1} Q_r(\Psi) \tag{13}$$

where u_r is the race deformation in radial direction at azimuth position ψ, Q_r is the radial component of the applied load at azimuth Ψ and K^{-1} is the inverse stiffness or compliance. The latter represents a complex non-linear relationship between load and deformation and depends on mechanical properties, azimuth position ψ of interest and the azimuth Ψ of the applied load. Based on the principle of superposition it is proposed to model the compliance by the use of a set of deformation shapes and related individual compliance approximation functions:

$$K^{-1} = \boldsymbol{\varphi}(\psi)\boldsymbol{\Theta}(\Psi) \tag{14}$$

where $\boldsymbol{\varphi}(\psi)$ is a column vector containing the set of normalized deformation shapes as function of azimuth position ψ and $\boldsymbol{\Theta}(\Psi)$ is a row vector containing the compliance approximation as function of azimuth Ψ of the applied load. The former is dimensionless and the latter is of dimension [m/N]. In the following two subsections the static deformation shape vector $\boldsymbol{\varphi}(\psi)$ and compliance vector $\boldsymbol{\Theta}(\Psi)$ will be defined respectively.

3.1. Static deformation shapes

The static deformation shapes define the deformation degrees of freedom of the bearing outer race. They allow for an effective and accurate representation of the normalized raceway deformation. A wavelike representation is proposed:

$$\boldsymbol{\varphi}(\psi) = \begin{bmatrix} \sin(\psi m)_{m=1} & \cdots & \sin(\psi m)_{m=M} & \cos(\psi m)_{m=1} & \cdots & \cos(\psi m)_{m=M} \end{bmatrix} \tag{15}$$

where each column represents a deformation shape as function of bearing azimuth position ψ. The number of deformation shapes is defined by M and can be set according to the detail of interest. A choice for (co)sinusoidal description with an integer wavelength is made as these are orthogonal and continuous (C^∞) over the entire bearing azimuth. The latter is important as the bearing elastic deformation should result in a continuous surface.

3.2. Compliance approximation

The compliance approximation is a vector composed of $2M$ compliance functions:

$$\boldsymbol{\Theta}(\Psi) = \begin{bmatrix} \theta_1(\Psi) \\ \vdots \\ \theta_{2M}(\Psi) \end{bmatrix} \tag{16}$$

where each compliance function $\theta_m(\Psi)$ describes the relationship between load Q at and the mth deformation degree of freedom. These functions depend on the location of the applied load and mechanical properties of the structure. To limit the function complexity only the load azimuth Ψ is considered whilst the effect of operating contact angle α is neglected. As the mechanical behaviour of a bearing can be considered periodic in nature, a Fourier series approximation is proposed to cast the properties of the compliance. The following description for each compliance function is proposed:

$$\theta_m(\Psi) = \frac{1}{2} a_{m,0} + \sum_{k=1..K} a_{m,k} \cos(k\Psi) + \sum_{k=1..K} b_{m,k} \sin(k\Psi) \tag{17}$$

where a_m and b_m are the Fourier coefficients for deformation shape m and K is the order of the Fourier series. The Fourier coefficients are determined a priori based on the real deformation behaviour of the outer race structure. For the latter a Finite Element study on the flexible structure is proposed.

By the use of a Finite Element Analysis the raceway deformation $u^{ref}(\psi,Q(\Psi))$ is determined after applying load Q at azimuth Ψ and nominal contact angle α_0. Now combining Eqs. (14)–(17) and substitution of $u_r(\psi)$ by $u^{ref}(\psi,Q(\Psi))$ one obtains:

$$\theta_m(\Psi) = \int_{-\pi}^{\pi} \frac{u^{ref}(\psi, Q(\Psi))}{\varphi_m(\psi) Q(\Psi)} d\psi \tag{18}$$

The equation provides the Fourier function values for all $2M$ compliance functions for a load at azimuth Ψ. Now by performing a Finite Element study for load Q at multiple azimuths ranging from $[-\pi < \Psi \leq \pi]$ standard Fourier theory can be applied to obtain the Fourier coefficients for all $2M$ compliance approximation functions.

3.3. Raceway deformation

The single load - deformation relationship presented can be extended to an arbitrary number of deformation locations N_{def} and rolling element loads N_{re} for a complete description of the raceway deformation. Eq. (19) shows how additional deformation locations (N_{def}) are added by extension of the static deformation shape vector/matrix with a row for each location of interest. Furthermore the amount of rolling element loads (N_{re}) can be increased by extending the compliance vector/matrix with extra columns and the load vector with additional rows.

$$\begin{bmatrix} u_r(\psi_1) \\ \vdots \\ u_r(\psi_{N_{def}}) \end{bmatrix} = \begin{bmatrix} \boldsymbol{\varphi}(\psi_1) \\ \vdots \\ \boldsymbol{\varphi}(\psi_{N_{def}}) \end{bmatrix} [\boldsymbol{\Theta}(\Psi_1) \quad \cdots \quad \boldsymbol{\Theta}(\Psi_{N_{re}})] \begin{bmatrix} Q_r(\Psi_1) \\ \vdots \\ Q_r(\Psi_{N_{re}}) \end{bmatrix} \tag{19}$$

3.4. Solution scheme for model solving

Due to the recursive dependency of the rolling element loads and raceway deformation an iterative approach is necessary for calculation of the rolling element and bearing loads for any chosen displacement vector. Fig. 3 presents the solution scheme for the proposed semi-analytical model.

The iterative nature rises due to the 'calculate load error ε' block that compares the current and previously calculated rolling element loads in order to determine convergence of the raceway deformation. The load error ε is the summation of the absolute rolling element load differences. When this error is smaller or equal to the tolerance threshold ε_{trs} the model has converged, otherwise a new calculation cycle is performed. This latter is always done during the first run as the convergence criterion cannot be checked then. The value ε_{trs} is chosen based on the desired accuracy. Note that the presented approach can be optimized for stability and convergence; this however is not focused upon in this paper.

4. Simulation based validation

The proposed model is validated by a comparison study with well-established SKF bearing simulation software [43–46]. More specifically, the accuracy of the rolling element load distribution of the semi-analytical model is assessed in a variety of load cases by comparison to results obtained by the SKF Bearing Simulation Tool (BEAST). Next to the validation with respect to the BEAST reference model also the differences with respect to a rigid model are considered to assess the improvement with respect to traditional modelling. This latter model is obtained by setting $M = 0$ which effectively corresponds to the rigid modelling presented in [1].

4.1. Study setup

The validation study considers a HBU3 bearing unit which is commonly used as wheel bearing in automotive applications. This double row angular contact ball bearing is designed to be light and compact. It provides its own housing and both the

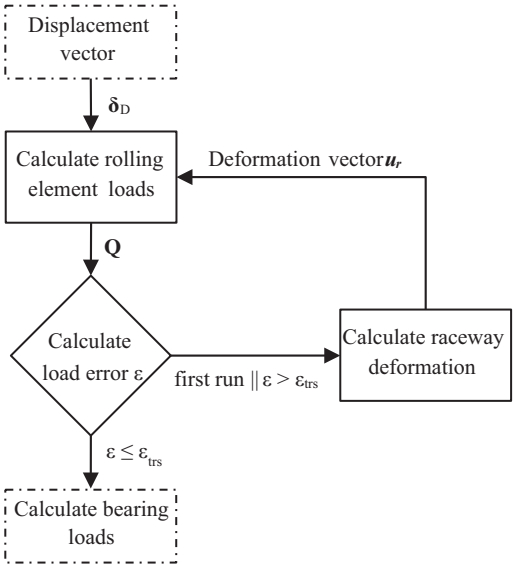

Fig. 3. Solution scheme for the flexible bearing model.

inner and outer-ring contain a flange for mounting to the wheel and knuckle respectively. The design considerations result in a relatively thin outer-ring which deforms considerably even at normal operating conditions. The bearing is therefore an ideal case study to assess the validity of the proposed model. Table 1 and Fig. 4 provide the relevant parameters of the considered bearing.

4.1.1. Semi-analytical model

The semi-analytical model is constructed according to Sections 2 and 3 by the use of the bearing parameters presented in Table 1. The model consists of two inner and outer raceways with the origin located as indicated in Fig. 4. The inner raceways are considered rigid and their groove curvature loci are described by displacement vector $\boldsymbol{\delta}_D$. The outer races are considered flexible. The bulk deformation of both in- and outboard raceways is assumed identical and thus is captured by a single set of deformation shapes.

The outer-ring geometry is modelled in a 3D CAD package and a Finite Element Analysis in COMSOL [47] is performed to determine the bearing deformation behaviour. As the knuckle to which the bearing is originally mounted is relatively flexible, spring connections at each of the bolt holes are chosen as boundary conditions. The stiffness of each of the bolt connections is determined by a FEA on the knuckle structure.

The reference deformation profile $u^{ref}(\psi)$ is determined in-between both raceways, as shown in Fig. 4, at a constant interval over the full bearing azimuth as indicated in Fig. 5. This latter figure also shows the azimuth interval distribution of the point load cases $Q(\Psi)$. The actual interval values are provided in Table 2. Note that each load $Q(\Psi)$ is applied individually whilst the FEA results of the 120 deformation points are used according to the procedure presented in Section 3 to determine the deformation model. In order to assess the effect of the number of deformation shapes on the model accuracy several model variants are determined with different values for M.

Table 1
Parameters of the double row ball bearing.

Parameter	Description	Value
N_{re}	Nr. rolling elements	2×15
r_i	Inner raceway groove curvature	6.59 mm
r_o	Outer raceway groove curvature	6.73 mm
R_{i0}	Inner raceway groove radius	33.19 mm
R_{o0}	Outer raceway groove radius	32.69 mm
Z_{i0}	Axial offset inner raceway	8.44 mm
Z_{o0}	Axial offset outer raceway	8.81 mm
D	Rolling element diameter	12.70 mm
α_0	Nominal contact angle	36° deg
R_{ref}	Reference profile radius	$R_o + r_o$
	Axial interference	30 μm

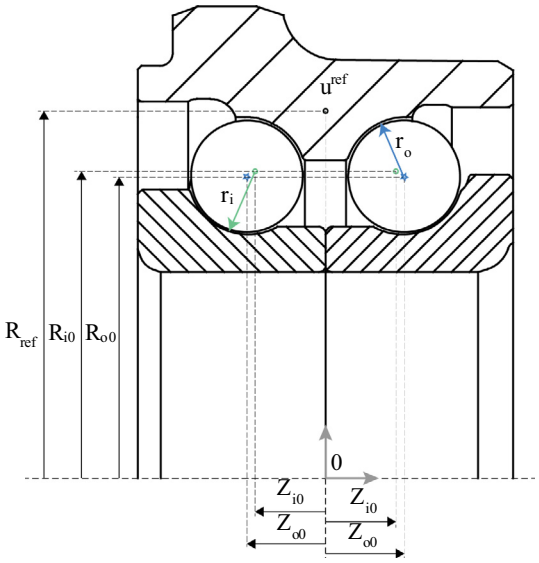

Fig. 4. Schematic view of HBU 3 bearing considered in this study.

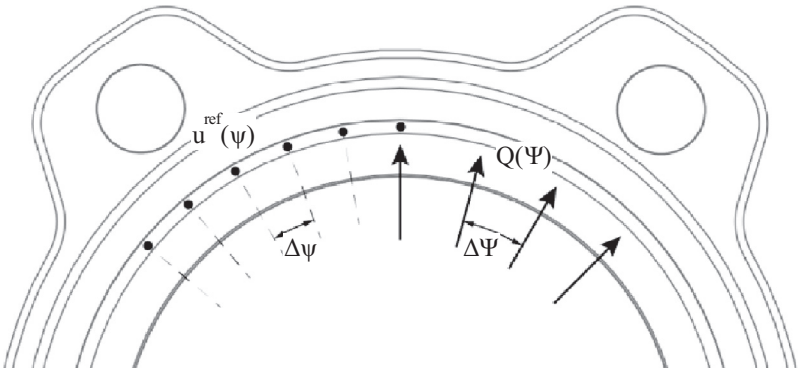

Fig. 5. Partial front view of the bearing outer ring showing the distribution of the deformation points and the individually applied point loads.

Table 2
Deformation and load parameters.

Parameter	Description	Value
$\Delta\psi$	Deformation profile azimuth interval	3° deg
$\Delta\Psi$	Load azimuth interval	5° deg

4.1.2. Reference study

As interest lies in the reconstruction of the rolling element load distribution for the purpose of real-time load monitoring it is chosen to use the SKF in-house multibody simulation software tool BEAST as a reference study. The choice for the BEAST software tool is related to its ability and efficiency for studying bearing behaviour of running bearings in the time domain. This is a result of the detailed and efficient contact analysis and parallelization of contact calculations over multiple processors for reduction of calculation times. Although by default bodies are considered rigid, BEAST allows for flexibility of all components based on a reduced mode shape representation of the deformation. For a detailed description of how this latter is handled in BEAST we refer the reader to [46]. The BEAST tool has been verified against finite element models and experiments and gives an exact solution for Hertzian contacts [43,44].

The model implemented in BEAST consists of inner ring, outer ring, 2×15 rolling elements and a cage in both inboard and outboard raceway. The outer ring is modelled as a flexible body by a model order reduction of the Finite Element mesh using a free interface method resulting in a total of 270 mode shapes. All other components are modelled as rigid. The inner-ring is rotated with constant speed and is loaded according to the provided input loads. As a rotating bearing is considered a settling period is taken in account for the system to reach steady state after which results are captured.

4.2. Simulation results

4.2.1. Single load case

This first set of load cases focuses on pure radial loading. In Fig. 6 the in- and outboard rolling element loads and operating contact angles for a 5 kN radial load case are presented for the proposed-, rigid- and reference BEAST model.

Considering the BEAST reference results, an almost symmetrical response with a peak force of approximately 800 N on both in- and outboard raceways can be observed. As the loading is relatively low the operating angles are close to nominal. A small difference between in- and outboard contact angles can be noted which relates to local bending of the outer race. It can be observed that entering ($\psi = -\pi$) and leaving ($\psi = \pi$) the loaded zone takes place at different contact angles.

Comparing the proposed $M = 4$ and rigid model with respect to the reference model it can be observed that the proposed model more accurately describes the rolling element loads. The flexible model peak force at zero azimuth is slightly lower whilst a slight increase of element loading is found at the sides of the bearing ($\psi = -\pi/2$ and $\psi = \pi/2$) with respect to the rigid model. The flexible model behaviour corresponds to the BEAST reference study as it allows for the bearing structure to deform oval as a response to the applied loading. The asymmetry in operating contact angles is not represented by the flexible (and rigid) model as the local effect causing it is not captured by the bulk deformation shapes.

A quantitative insight in the accuracy of the proposed flexible model, including the effect of the number of deformation shapes, is provided by Table 3. The table presents the rolling element load distribution root-mean-square error (RMSE) values of the rigid and the proposed model ($M = [1, 2, 3, 4, 6, 10]$) with respect to the reference model for four different load cases.

As observed in the qualitative analysis the table shows that the proposed model provides a more accurate description of the rolling element loads than the traditional rigid model. Results indicate that the first deformation shapes corresponding to $M = 1$ have no effect, however a significant accuracy improvement is observed with $M = 2$ and $M = 3$ as RMS errors decrease

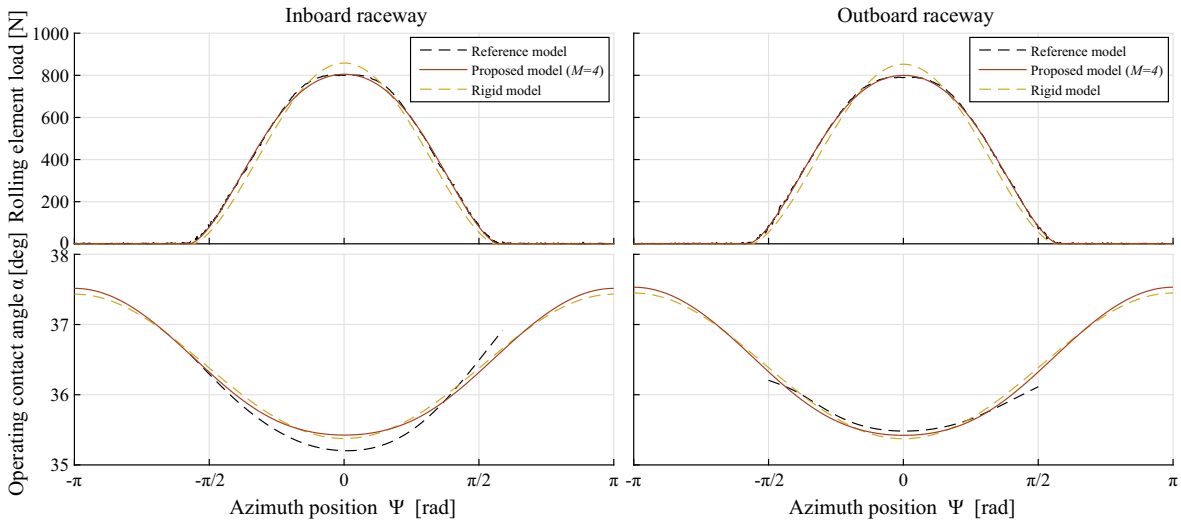

Fig. 6. In- and outboard rolling element load distribution and corresponding operating angles for the BEAST reference, proposed ($M = 4$) and rigid model for an applied radial bearing load of 5 kN.

Table 3
RMSE values of the rolling element load distribution for four different single load cases.

Applied load	Model variant						
Fx	Rigid	M = 1	M = 2	M = 3	M = 4	M = 6	M = 10
3 kN	15 N	15 N	7 N	5 N	5 N	5 N	5 N
4 kN	22 N	22 N	9 N	5 N	5 N	5 N	5 N
5 kN	30 N	30 N	10 N	6 N	6 N	6 N	6 N
6 kN	38 N	38 N	13 N	8 N	8 N	7 N	7 N

by an average of 62% and 75% respectively. Further increasing the number of static deformation mode shapes seems not to significantly improve the accuracy any further. A relative improvement of the RMS error between $M = 10$ and rigid model of respectively 68%, 77%, 80% and 80% is found for the 3 kN, 4 kN, 5 kN and 6 kN load cases.

4.2.2. Combined load case

This second set of load cases focuses on combined loading situations. Fig. 7 presents the rolling element loads and operating contact angles based on the proposed-, rigid- and reference BEAST model for a 5 kN radial, 4 kN axial and 1.2 kNm moment combined load case.

The applied moment results in opposing azimuth positions for the in- and outboard peak loads. As the radial force is applied in positive x-direction the outboard peak load is considerably higher than inboard peak load. The axial bearing force furthermore causes the inboard load distribution to be significantly wider than the outboard counterpart. Considering the operating contact angles it is observed that the combined load causes significant differences between in- and outboard raceway. Especially the inboard contact angle deviates considerably from the nominal angle.

Comparing the proposed and rigid model with respect to the reference model it can be observed that the proposed model is considerably more accurate. While the rigid model significantly overestimates the peak loads, these are accurately described by the proposed model. Next to that also the load distribution at the sides of the bearing is better represented by the proposed model. In line with the pure radial loading case the improved accuracy by the proposed model is related to the oval deformation of the bearing due to the applied load. For the operating contact angles we see a slight improvement using the proposed model although errors up to 1.5 deg are observed at the peak loads.

Table 4 provides the rolling element load distribution RMSE values for four different combined load cases. As in previous section the rigid- and proposed model results are compared to the BEAST reference model.

In line with the results of the single load test cases it can be observed that increasing the number of deformation shapes improves the accuracy of the rolling element load distribution. Again it is observed that the deformation shapes related to $M = 1$ do not have any effect whilst up to the $M = 6$ model considerable improvements are found. The deformation shapes related to $M = 2$ provide most significant improvement as RMS errors decrease by an average of 62%. The $M = 10$ case shows a slight decrease in accuracy compared to $M = 6$. Comparing the relative RMS error between $M = 6$ and rigid model an improvement of respectively 78%, 68%, 69% and 76% is found for the 1.5 kNm, 0.9 kNm, −0.9 kNm and −1.5 kNm cases.

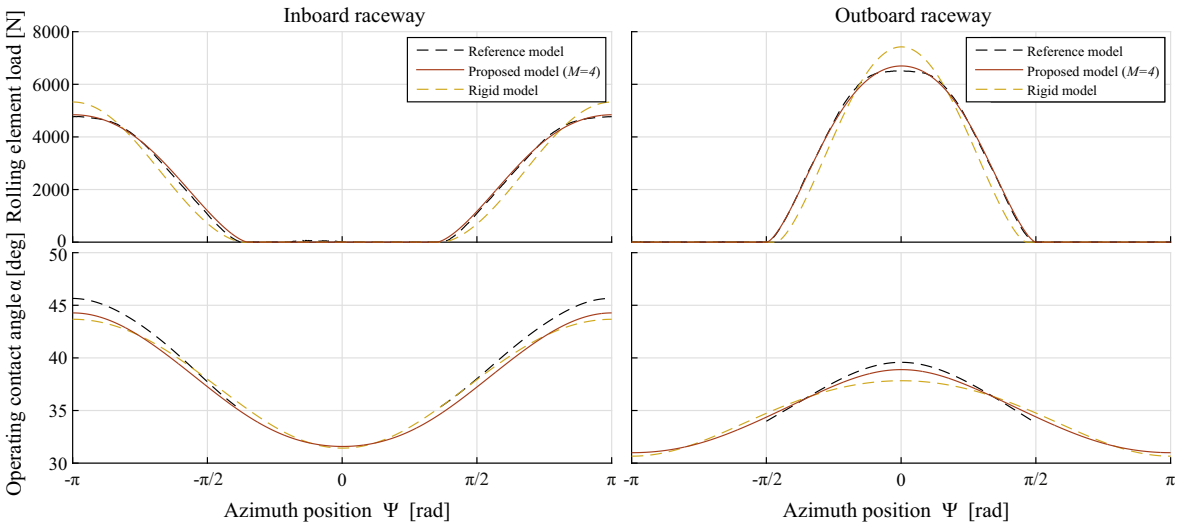

Fig. 7. In- and outboard rolling element load distribution and corresponding operating angles for the BEAST reference, proposed ($M = 4$) and rigid model for a combined load case.

Table 4
RMSE values of the rolling element load distribution for combined loading conditions.

Applied load			Model variant						
Fx	Fz	Mx	Rigid	M = 1	M = 2	M = 3	M = 4	M = 6	M = 10
4.9 kN	5.1 kN	1.5 kNm	424 N	424 N	139 N	120 N	98 N	92 N	92 N
5.0 kN	2.9 kN	0.9 kNm	232 N	232 N	110 N	90 N	77 N	74 N	74 N
5.0 kN	−2.9 kN	−0.9 kNm	214 N	214 N	89 N	87 N	72 N	66 N	67 N
4.9 kN	−5.1 kN	−1.5 kNm	423 N	423 N	136 N	137 N	111 N	100 N	101 N

4.3. Discussion

Both sets of load cases show that the proposed model provides a more accurate rolling element load distribution than the traditional rigid model for the analysed bearing. For both load cases it is found that heavier load conditions result in more improvement in both absolute as relative sense. This can be explained as these test cases result in more deformed structures, and thus considering deformation effects is more advantageous.

With respect to the effect of the number of deformation shapes it is clearly observed that the deformation shapes corresponding to $M = 1$ are insignificant and thus do not reflect any occurring real deformation. The deformation shapes corresponding to $M = 2$ result in most significant improvement and slight improvements are observed until $M = 4$ for the single load cases and $M = 6$ for the combined load cases. Most probably this pattern is representative for most cases, as in general the first mode shapes take in account for the bulk of deformation. However this depends on the geometry and boundary conditions of the structure. The results furthermore show that in more complex loading combinations it is advantageous to take in account more deformation shapes.

In general it can thus be concluded that the flexibility model results in a significantly better description of the rolling element load distribution. The absolute improvement however is case dependent as geometry, mechanical properties, boundary conditions and loading affect the results.

5. Experimental study

In the following an experimental study is presented that applies the flexible bearing model in a novel bearing load condition monitoring approach. It shows the potential of the proposed model when combined with the rolling element load reconstruction approach presented in [23,26].

5.1. Proposed bearing load condition monitoring approach

A strain gauge instrumented bearing is used to determine both in- and outboard rolling element loads at several azimuth positions using the approach presented in [26]. Based on the measured rolling element loads the proposed bearing model can be used to reconstruct the bearing loading. This is achieved by finding the displacement vector δ_D that minimizes the error

between the measured and modelled rolling element loads. As the proposed flexible bearing model provides a more accurate relationship between rolling element and bearing loading better results can be expected with respect to usage of a rigid model.

5.2. Experimental setup

The outer-ring of an automotive HBU3 bearing unit, one identical to the discussed bearing is Section 4, is instrumented with eight strain gauges at four orthogonal azimuth positions. Fig. 8 shows a top view of the bearing in which the top two strain gauges, covered by a protective layer, can be observed. The bearing is mounted in a dedicated bearing test rig, shown in Fig. 9, which allows for static and dynamic load cases at various speeds. The operating range of the test bench is presented in Table 5. In the current study static load cases are applied at a rotational speed of ω = 1000 rpm. A *Yokogawa* data logger is used to capture the conditioned strain gauge information at a sampling frequency of 2 kHz. The proposed load conditioning approach is applied off-line.

5.3. Results

5.3.1. Case I: Radial and moment loading

This load case considers a combination of a radial load of 5 kN and applied moment of approximately 1 kNm. Fig. 10 shows the estimated rolling element loads at the four strain measurement azimuths and the reconstructed rolling element load distribution by both proposed flexible and rigid bearing model.

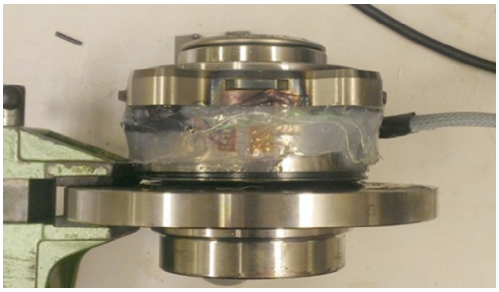

Fig. 8. Instrumented HBU3 bearing unit.

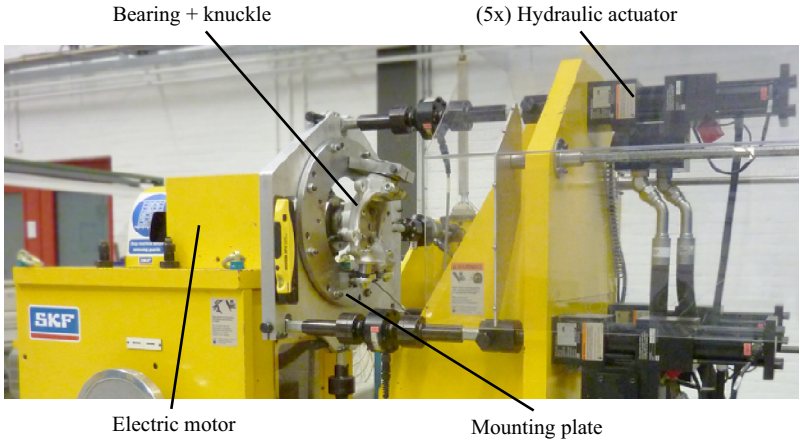

Fig. 9. Bearing test rig at SKF which is used for the experimental study.

Table 5
Test rig operating specifications.

Radial load	F_x	±15 kN
Radial load	F_y	±15 kN
Axial load	F_z	±15 kN
Moment load	M_x	±5 kNm
Moment load	M_y	±5 kNm
Rotational speed	ω	0–3000 rpm

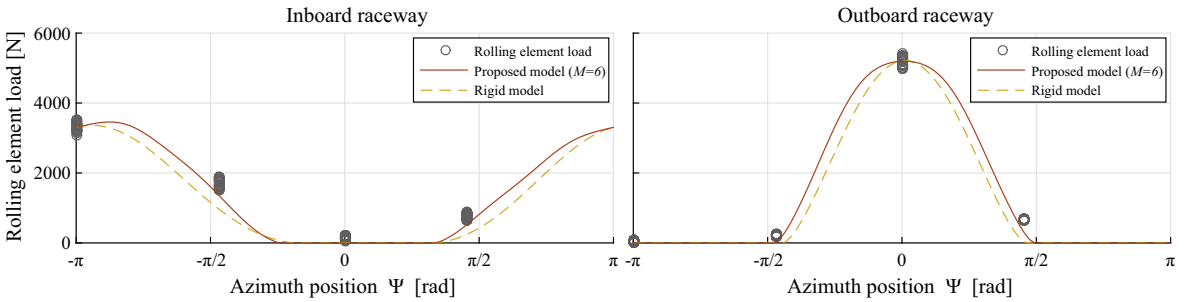

Fig. 10. Reconstruction results of load case I presenting the estimated rolling element loads and fitted load distributions.

Table 6
Applied and estimated loads of load case I based on the proposed flexible ($M = 6$) and rigid model.

	Fx	Fy	Fz	Mx	My
Applied load	4.9 kN	−0.7 kN	0.0 kN	−0.1 kNm	0.9 kNm
Proposed model ($M = 6$)	5.0 kN	−1.7 kN	0.4 kN	−0.1 kNm	0.9 kNm
Rigid model	4.4 kN	−1.6 kN	0.3 kN	−0.1 kNm	0.8 kNm

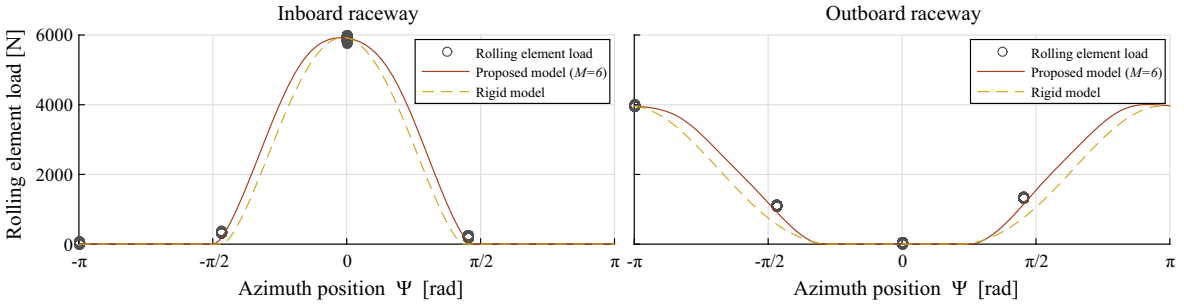

Fig. 11. Results of test case II showing estimated rolling element loads and fitted load distributions.

Table 7
Applied and estimated loads of load case II based on the proposed ($M = 6$) and rigid model.

	Fx	Fy	Fz	Mx	My
Applied load	4.9 kN	−0.7 kN	−2.0 kN	−0.1 kNm	−1.0 kNm
Proposed model (M = 6)	5.0 kN	0.2 kN	−1.5 kN	−0.1 kNm	−1.0 kNm
Rigid model	4.5 kN	0.2 kN	−1.1 kN	−0.1 kNm	−0.9 kNm

Multiple load estimates for all bearing azimuths can be observed in Fig. 10 as a brief period of time is considered in order to minimize the effect of noise in the rolling element load estimates. Regarding the rolling element load reconstruction using both models it can be clearly seen that the proposed flexible model is better able to match the load estimates. The more slim rolling element distribution obtained using the rigid model is not able to capture the element loads at the side of the bearing. This latter relates to the inability to capture the oval deformation of the bearing.

The load estimates based on the proposed and rigid model in this test case are presented in Table 6.

The quantitative results show that the approach is well able to reconstruct the bearing loading using both flexible and rigid model, where the flexible model is slightly more accurate. Both moment loads are accurately reconstructed although the approach results in significant errors in estimating radial load F_y and axial load F_z. The flexible model provides a significantly better estimate for the radial F_x load.

5.3.2. Case II – Radial, axial and moment loading

In this second experimental load case a radial load of about 5 kN, axial load of −2 kN and moment of approximately −1 kN is applied. The rolling element load distribution results of this experiment are presented in Fig. 11.

In accordance with load case I it is observed that the proposed model is better able to fit the estimated rolling element loads. The rigid model again results in a too slim load distribution being unable to fit all rolling element loads. Table 7 presents the load reconstruction results of both models.

The presented results again show good accuracy of the load monitoring approach by both models. As for load case I, the proposed model outperforms the rigid model based approach. Both moment loads are well estimated, radial load F_y and axial load F_z provide significant errors and radial load F_x is approximated better by the flexible model. This all is in line with the results of load case I.

5.4. Discussion

The proposed bearing load condition monitoring approach is able to provide good estimates of the bearing loading using both the rigid as well as the flexible model. Results show better estimates by the use of the proposed model, which is in line with expectations as it is shown in Section 4 that the proposed model provides a more accurate relationship between rolling element loads and bearing loading.

As the two test cases only represent a small sample of all possible load conditions the results do not prove global validity of the approach. However, it does show its potential for load condition monitoring. The two test cases show that both moment loads can be well estimated whilst radial and axial loads sometimes show considerable errors. The proposed bearing model shows better performance, especially for the radial F_x load case. This latter is backed up by the simulation study of Section 4.2.1 which also showed that the radial peak load was much better captured by the flexible model.

Lastly it must be noted that the errors in the bearing load estimates can also be related to errors in the reconstructed rolling element loads, as the approach used [26] is still under development.

6. Conclusion

The paper presents a semi-analytical bearing model that addresses flexibility of the bearing outer race structure. By combining static deformation shapes and a Fourier series based compliance approximation an accurate description of the deformation of the raceway structure is obtained. A comparison study to a well-established bearing simulation tool shows that the proposed model outperforms traditional rigid bearing models for all loading conditions in case of a flexible outer raceway structure. The model accuracy depends on the number of static deformation shapes considered. For the case study it is found that the first set of relevant deformation shapes results in an average decrease of rolling element load distribution RMS errors of 62%, whilst an improvement of up to 80% can be obtained when a higher number of shapes is taken in account. In contradiction to other bearing models considering raceway flexibility the proposed model is of low computational costs and provides no limitations on the structure geometry making it applicable for real-time applications. An experimental application study furthermore shows that in combination with earlier work of the authors the model shows high potential with respect to bearing load monitoring as it allows for the reconstruction of all 5 relevant bearing loads.

Acknowledgments

The research leading to these results has received funding from the European Union Horizon 2020 Framework Program, Marie Sklodowska-Curie actions, under grant agreement no. 645736. Furthermore the authors would like to thank their industrial partner SKF for the support provided.

References

[1] T. Harris, Rolling Bearing Analysis, John Wiley and sons, 2001.
[2] ISO, 15243: 2004 Rolling Bearings—Damage and Failures—Terms, Characteristics and Causes, British Standards Institution, 2004.
[3] T. Williams, X. Ribadeneira, S. Billington, T. Kurfess, Rolling element bearing diagnostics in run-to-failure lifetime testing, Mech. Syst. Signal Process. 15 (2001) 979–993.
[4] T. Liu, J. Mengel, Intelligent monitoring of ball bearing conditions, Mech. Syst. Signal Process. 6 (1992) 419–431.
[5] N. Tandon, A. Choudhury, A review of vibration and acoustic measurement methods for the detection of defects in rolling element bearings, Tribol. Int. 32 (1999) 469–480.
[6] I. El-Thalji, E. Jantunen, A summary of fault modelling and predictive health monitoring of rolling element bearings, Mech. Syst. Signal Process. 60–61 (2015) 252–272.
[7] H. de Azevedo, A. Araújo, N. Bouchonneau, A review of wind turbine bearing condition monitoring: State of the art and challenges, Renew. Sustain. Energy Rev. 56 (2016) 368–379.
[8] J. Lee, F. Wu, W. Zhao, M. Ghaffari, L. Liao, D. Siegel, Prognostics and health management design for rotary machinery systems—Reviews, methodology and applications, Mech. Syst. Signal Process. 42 (2014) 314–334.
[9] C. Peeters, P. Guillaume, J. Helsen, A comparison of cepstral editing methods as signal pre-processing techniques for vibration-based bearing fault detection, Mech. Syst. Signal Process. 91 (2017) 354–381.
[10] B. Dolenc, P. Boškoski, Đ. Juričić, Distributed bearing fault diagnosis based on vibration analysis, Mech. Syst. Signal Process. 66–67 (2016) 521–532.
[11] S. Ericsson, N. Grip, E. Johansson, L. Persson, R. Sjöberg, J. Strömberg, Towards automatic detection of local bearing defects in rotating machines, Mech. Syst. Signal Process. 19 (2005) 509–535.
[12] B. Muruganatham, M. Sanjith, B. Krishnakumar, S. Satya Murty, Roller element bearing fault diagnosis using singular spectrum analysis, Mech. Syst. Signal Process. 35 (2013) 150–166.
[13] A. Morhain, D. Mba, Bearing defect diagnosis and acoustic emission, Proc. Inst. Mech. Eng., Part J: J. Eng. Tribol. 217 (2003) 257–272.
[14] W. Caesarendra, B. Kosasih, A. Tieu, H. Zhu, C. Moodie, Q. Zhu, Acoustic emission-based condition monitoring methods: Review and application for low speed slew bearing, Mech. Syst. Signal Process. 72–73 (2016) 134–159.
[15] X. Zhu, C. Zhong, J. Zhe, Lubricating oil conditioning sensors for online machine health monitoring–a review, Tribol. Int. (2017).
[16] S. Bagavathiappan, B. Lahiri, T. Saravanan, J. Philip, T. Jayakumar, Infrared thermography for condition monitoring – A review, Infrared Phys. Technol. 60 (2013) 35–55.

[17] G. Lim, Y. Ali, B. Yang, The fault diagnosis and monitoring of rotating machines by thermography, in: Engineering Asset Management and Infrastructure Sustainability: Proceedings of the 5th World Congress on Engineering Asset Management, Springer London, London, 2012, pp. 557–565.
[18] A. Nembhard, J. Sinha, A. Pinkerton, K. Elbhbah, Combined vibration and thermal analysis for the condition monitoring of rotating machinery, Struct. Health Monit. 13 (2014) 281–295.
[19] Z. Peng, N. Kessissoglou, An integrated approach to fault diagnosis of machinery using wear debris and vibration analysis, Wear 255 (2003) 1221–1232.
[20] S. Kerst, B. Shyrokau, E. Holweg, Anti-lock Braking Control based on Bearing Load Sensing, Presented at the EuroBrake, Dresden, Germany, 2015.
[21] H. Mol, Method and sensor arrangement for load measurement on rolling element bearing based on model deformation, US Patent 7389701, 2008.
[22] K. Nishikawa, Hub bearing with integrated multi-axis load sensor, Techn. Rev. (2011).
[23] S. Kerst, B. Shyrokau, E. Holweg, Reconstruction of wheel forces using an intelligent bearing, SAE Int. J. Passenger Cars-Electron. Electr. Syst. 9 (2016) 196–203.
[24] M. Kraus, M. Bäuml, Continuous wheel force measurement for passenger vehicles and commercial vehicles, in: 6th International Munich Chassis Symposium, Munich, Germany, 2015, pp. 717–717.
[25] A. Reedman, H. Yang, Bearing Monitoring Using a Fibre Bragg Grating, Google Patents, 2014.
[26] S. Kerst, B. Shyrokau, E. Holweg, Wheel force measurement for vehicle dynamics control using an intelligent bearing, in: Advanced Vehicle Control AVEC16, CRC Press, 2016, pp. 547–552.
[27] L. Rasolofondraibe, B. Pottier, P. Marconnet, X. Chiementin, Capacitive sensor device for measuring loads on bearings, IEEE Sens. J. 12 (2012) 2186–2191.
[28] J. Den Engelse, Estimation of the Lateral Force, Acting at the Tire Contact Patch of a Vehicle Wheel, Using a Hub Bearing Unit Instrumented with Strain Gauges and Eddy-current Sensors, Delft University of Technology, 2013.
[29] K. Ono, T. Takizawa, M. Aoki, Preload measuring device for double row rolling bearing unit, US Patent 8864382, 2014.
[30] A. Madhusudhanan, M. Corno, M. Arat, E. Holweg, Load sensing bearing based road-tyre friction estimation considering combined tyre slip, Mechatronics 39 (2016) 136–146.
[31] J. Van Doornik, Haptic Feedback on the Steering Wheel Near the Vehicle's Handling Limits Using Wheel Load Sensing, Delft University of Technology, 2014.
[32] B. Leeuwen, J. Zuurbier, Vehicle state estimation based on load sensing, presented at the Vehicle Dynamics Expo, 2007.
[33] J. de Mul, J. Vree, D. Maas, Equilibrium and associated load distribution in ball and roller bearings loaded in five degrees of freedom while neglecting friction—Part I: general theory and application to ball bearings, J. Tribol. 111 (1989) 142–148.
[34] A. Jones, A general theory for elastically constrained ball and radial roller bearings under arbitrary load and speed conditions, ASME J. Basic Eng. 82 (1960) 309–320.
[35] A. Bourdon, J. Rigal, D. Play, Static rolling bearing models in a CAD environment for the study of complex mechanisms: Part I—Rolling bearing model, J. Tribol. 121 (1999) 205–214.
[36] S. Lacroix, D. Nélias, A. Leblanc, Four-point contact ball bearing model with deformable rings, J. Tribol. 135 (2013) 031402.
[37] J. Fiszer, T. Tamarozzi, B. Blockmans, W. Desmet, A time-dependent parametric model order reduction technique for modelling indirect bearing force measurements, Mech. Mach. Theory 83 (2015) 152–174.
[38] A. Daidié, Z. Chaib, A. Ghosn, 3D simplified finite elements analysis of load and contact angle in a slewing ball bearing, J. Mech. Des. 130 (2008) 082601.
[39] C. Wagner, A. Krinner, T. Thümmel, D. Rixen, Full dynamic ball bearing model with elastic outer ring for high speed applications, Lubricants 5 (2017) 17.
[40] A. Leblanc, D. Nélias, C. Defaye, Nonlinear dynamic analysis of cylindrical roller bearing with flexible rings, J. Sound Vib. 325 (2009) 145–160.
[41] C. Defaye, D. Nélias, A. Leblanc, F. Bon, Theoretical analysis of high-speed cylindrical roller bearing with flexible rings mounted in a squeeze film damper, Tribol. Trans. 51 (2008) 762–770.
[42] G. Cavallaro, D. Nélias, F. Bon, Analysis of high-speed intershaft cylindrical roller bearing with flexible rings, Tribol. Trans. 48 (2005) 154–164.
[43] L. Stacke, D. Fritzson, P. Nordling, BEAST—a rolling bearing simulation tool, Proc. Inst. Mech. Eng., Part K: J. Multi-body Dynam. 213 (1999) 63–71.
[44] L. Stacke, D. Fritzson, Dynamic behaviour of rolling bearings: simulations and experiments, Proc. Inst. Mech. Eng., Part J: J. Eng. Tribol. 215 (2001) 499–508.
[45] I. Nakhimovski, Contributions to the Modeling and Simulation of Mechanical Systems with Detailed Contact Analyses, Linköping University Electronic Press, 2006.
[46] I. Nakhimovski, Modeling and Simulation of Contacting Flexible Bodies in Multibody Systems, Institutionen för datavetenskap, 2002.
[47] COMSOL multiphysics user's guide, Version: September, vol. 10, 2005, pp. 333.